Dynamic response of molybdenum shock compressed at 1400 °C

Thomas S. Duffy[a] and Thomas J. Ahrens
Lindhurst Laboratory of Experimental Geophysics, Seismological Laboratory, California Institute of Technology, Pasadena, California 91125

(Received 23 December 1993; accepted for publication 24 March 1994)

Wave profile measurements are reported for pure molybdenum initially heated to 1400 °C and shock compressed to stresses between 12 and 81 GPa. The Hugoniot states are consistent with previous results and all data can be described by the parameters: $c_0=4.78(2)$ km/s and $s=1.42(2)$, where the numbers in parentheses are one standard deviation uncertainties in the last digits. The amplitude of the Hugoniot elastic limit is 1.5–1.7 GPa at 1400 °C compared with 25 °C values of 2.3–2.8 GPa. Unloading wave velocities range from 6.30(22) km/s at 12.0 GPa to 7.91(24) km/s at 80.7 GPa and are 4%–8% below extrapolated ultrasonic values and Hugoniot measurements from a room temperature initial state. These differences can be explained by the effect of temperature on the compressional elastic wave velocity. No temperature dependence of the dynamic tensile strength can be resolved from the present data.

I. INTRODUCTION

Wave profile measurements on materials shock compressed at high initial temperature can provide insights into the effect of temperature on elastic, constitutive, and equation of state (EOS) properties. Velocity interferometric techniques[1] are the standard method for probing the detailed response of metals and minerals to shock compression. In this study, we extend the range of such measurements to materials at very high initial temperatures.

Molybdenum (Mo) was chosen for study because of its role as a high-pressure standard. There has been much interest in the dynamic behavior of this material.[2–4] The EOS of Mo at 1400 °C has been studied recently by shock transit time measurements.[5] Molybdenum is used as a containment material in EOS studies of liquid silicates,[6] and it is therefore desirable to fully characterize its high-temperature dynamic response. This material has also been compressed statically to 272 GPa at room temperature.[7] Detailed understanding of thermal and strength effects is required to relate shock and static data. Finally, sound velocities measured on Mo shock compressed from room temperature reveal complex behavior at stresses above 150 GPa which appear to reflect changes in bonding character.[8,9]

Material strength has been observed to decrease at high stress and high temperature in aluminum,[10] and many constitutive models include a thermal softening effect.[11] However, there is little quantitative information on the effect of temperature upon constitutive properties. The effect of high initial temperature on the strength of Mo is addressed in the present study.

II. EXPERIMENTAL TECHNIQUE

Dynamic compression of molybdenum was carried out by high-velocity plate impact. Foam-backed aluminum 6061 and tantalum flyer plates were mounted in lexan projectiles and accelerated to high velocities using a single-stage 40-mm bore propellant gun.[12] Projectile velocities were measured to ±1% by recording two x-ray shadowgraphs of the projectile in flight (10–50 μs apart) just prior to impact.

Molybdenum samples were machined from rods of polycrystalline stock of better than 99.95% purity (Climax Performance Materials Co.). The samples were cut into a top-hat shape as shown in Fig. 1 with an outer diameter of 44.5 mm and an inner diameter of 25.4 mm. The rear surface was lapped to a diffusely reflecting finish using 5-μm alumina powder. Crystal densities were measured by the Archimedean method and are consistent with the density of molybdenum determined by x-ray diffraction of 10.22 g/cm^3 (Table I).

The sample was mounted in a ceramic holder in the gun tank. A water-cooled copper coil positioned around the inner disk was connected to a 10-kW radio-frequency source which acted as an induction heater. Temperatures were measured using a Pt–Pt10%Rh thermocouple attached to the sample. Details of the sample heating procedure are described elsewhere.[5,6] The impact conditions are listed in Table I.

The motion of the molybdenum free surface was monitored using a VISAR (velocity interferometer system for any reflector) apparatus.[1] Light from an Ar^+ laser was focused onto the Mo rear surface using a lens and turning mirror (Fig. 1). The mirror was shielded from the thermal radiation of the sample by a ceramic shutter which was retracted pneumatically immediately prior to firing the gun. The diffusely reflected light, which is Doppler-shifted due to sample motion, is directed to the VISAR system where it is split into two legs of a wide-angle Michelson interferometer. The light in one leg is delayed in time by passing it through a length of fused silica, and the two beams produce interference fringes when recombined. The free surface velocity, u_{fs}, is related to the number of interference fringes by

$$u_{fs}(t-\tau/2)=kF(t), \tag{1}$$

where t is the time, τ is the delay time of the interferometer, $F(t)$ is the number of fringes, and k is the velocity-per-fringe constant. A fringe constant of 225 m/s/fringe was used for

[a]Present address: Geophysical Laboratory, 5251 Broad Branch Rd. NW, Washington, DC 20015.

 0021-8979/94/76(2)/835/8/$6.00

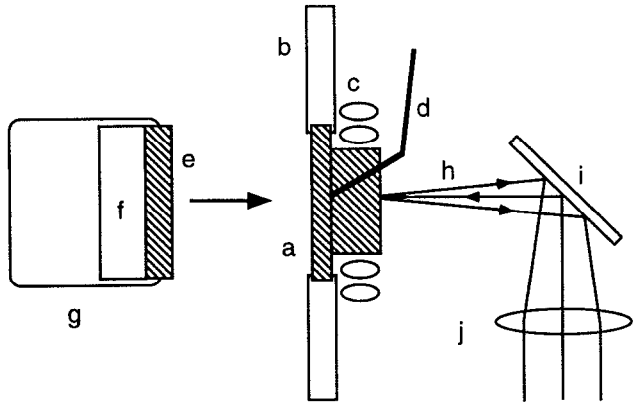

FIG. 1. Set-up for high-temperature VISAR experiments. The molybdenum sample (a) is held by a ceramic target plate (b) and radiatively heated to ~1400 °C using copper coils (c) attached to a 10-kW radio-frequency source acting as an induction heater. Temperature is measured by the thermocouple (d). The impactor assembly consists of a flyer plate (e) with foam backing (f) mounted in a lexan body (g). The free surface of the hot Mo sample is monitored with single-frequency light from a 3 W Ar^+ laser which is focused using the lens (j) and directed onto the target by the expendable mirror (i). The reflected light (h) is returned to the VISAR along a path parallel to the incident beam.

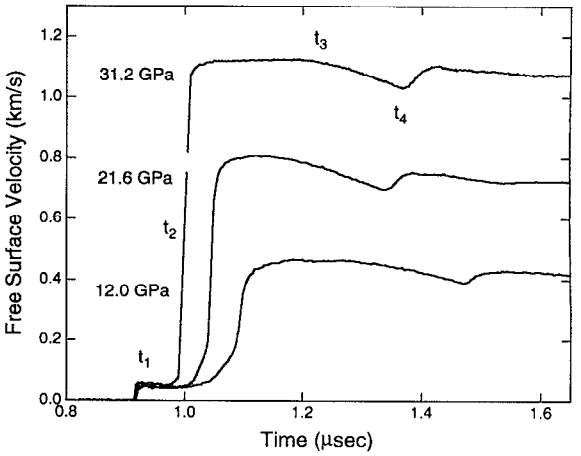

FIG. 2. Free surface velocity profiles measured on 1400 °C molybdenum samples. The starting times of the waveforms are arbitrary. The peak shock stresses are listed to the left of the profiles. The times t_1–t_4 correspond to the arrival times shown on the distance-time diagram of Fig. 3.

the present experiments. Fringe records were converted to velocity histories using an interactive data-reduction procedure.[13]

Due to the high-temperature sample environment, electrical shorting pins could not be used for triggering and tilt diagnostics. Instead, a trigger signal was generated by the interruption of a continuous laser beam which propagated across the projectile path 5 cm in front of the target. Due to the long time window between triggering and data acquisition, oscilloscope (Hewlett-Packard 54111D) sampling rates between 250–500 megasamples per second were used with a sampling window of 16–32 μs.

The sample reflectivity did not change significantly when heated to 1400 °C for ~15 minutes in the <100-μm Hg air pressure of the impact tank. Despite the use of a narrow bandpass filter, thermal radiation from the hot sample produced ~30 mV offsets in the fringe records which were subtracted in the data reduction process.

III. RESULTS

A. Wave profiles

Four experiments were conducted on Mo samples, three of which yielded free surface velocity profiles. In the fourth experiment, data recording failures prevented a wave profile from being obtained but the arrival times of the shock front and the initial unloading wave could be read directly from the partial fringe records. The velocity profiles are shown in Fig. 2.

The distance-time diagram of Fig. 3 illustrates the main features of the wave profiles. Impact at $t=0$ produces an elastic precursor and plastic shock which propagate through the sample and reach the free surface at times t_1 and t_2, respectively. The reflection of the shock at the free surface produces a rarefaction fan propagating back to the left. In the meantime, a shock travels through the thin flyer and reflects from the low-impedance backing layer, producing a forward-propagating rarefaction fan. For an elastic-plastic material, the velocity of the head of the rarefaction fan corresponds to the compressional sound velocity.[14] The lead characteristics of the two fans intersect at a distance h^* from the free surface. The forward-propagating unloading wave then reaches

TABLE I. Initial conditions for high-temperature VISAR experiments. ρ_0 is the initial density, T_0 is the initial temperature (±1 °C), and U_{fp} is the impact velocity. The numbers in parentheses are one standard deviation uncertainties in the last digit(s).

	Flyer			Sample			
Shot	Material	ρ_0 (g/cm^3)	Thickness (mm)	ρ_0 (25 °C) (g/cm^3)	Thickness (mm)	T_0 (°C)	U_{fp} (km/s)
865	Al 6061	2.688(12)	1.525(5)	10.210(6)	5.538(3)	1403	0.95(1)
866	Al 6061	2.692(8)	1.464(5)	10.204(6)	5.535(5)	1413	1.57(1)
867	Al 6061	2.699(7)	1.984(5)	10.197(5)	5.565(5)	1418	2.16(2)
868	Ta	16.58(7)	1.103(4)	10.208(6)	5.553(6)	1411	2.28(2)

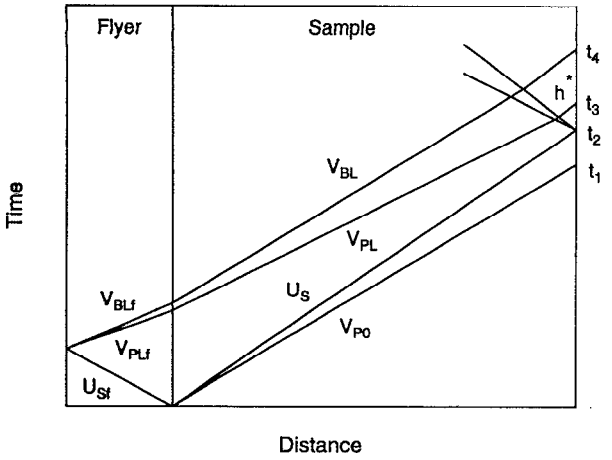

FIG. 3. Lagrangian distance-time diagram for the 21.6 GPa experiment of the previous figure. V_{P0} is the elastic precursor velocity, U_S is the shock velocity, V_{PL} and V_{BL} are the Lagrangian compressional and bulk velocities, respectively.

the free surface at t_3. The interaction of the two unloading waves leads to spall and produces the velocity pull-back seen in Fig. 2 (t_4).

B. Hugoniot states

A time reference for the experiments was established from the arrival time of the elastic precursor, which is assumed to travel with the ambient-pressure, high-temperature compressional sound velocity, V_{P0}. This assumption is reasonable given the relatively low elastic limit of molybdenum. The compressional sound velocity was determined by extrapolating the linear elastic modulus-temperature trend observed to 700 °C in ultrasonic data,[15] yielding $V_{P0}=6.11(3)$ km/s. The shock wave arrival was taken to be the midpoint between the peak Hugoniot elastic limit (HEL) velocity and the peak free surface velocity. For the three experiments shown in Fig. 2, the shock velocity, U_S, was then calculated from the sample thickness. The particle velocity behind the shock front, u_p, was determined from the measured free surface velocity by accounting for the elastic–plastic interaction at the free surface:[16]

$$u_p=\frac{1}{2}\left[u_{\rm fs}+\frac{(V_{P0}-V_{B0})\sigma_{\rm HEL}}{\rho_0 V_{P0}V_{B0}}\right], \tag{2}$$

where V_{B0} is the ambient-pressure bulk sound velocity, ρ_0 is the initial high-temperature density,[5] and $\sigma_{\rm HEL}$ is the elastic precursor amplitude discussed in the next section. The Hugoniot stresses and densities were then determined by application of the Rankine–Hugoniot conservation equations.[17] The Hugoniot states are shown in Table II and Fig. 4. The present results are in excellent agreement with previous data from shock transit time measurements.[5] The combined Hugoniot equation of state for 1400 °C Mo is given by:

$$U_S=4.78(2)+1.42(2)u_p, \tag{3}$$

where the numbers in parentheses are one standard deviation uncertainties. This EOS is only slightly different from previous work[5] but the formal uncertainties are reduced by factor of 2.5–3 and the equation of state is now constrained between 12 and 96 GPa.

TABLE II. 1400 °C molybdenum Hugoniot states. Results are from measured wave profiles except for experiment 868, in which case the measured flyer velocity and impedance matching were used to calculate the Hugoniot state. σ is the stress, and ρ is the density.

Shot	u_p (km/s)	U_S (km/s)	σ (GPa)	ρ (g/cm^3)
865	0.236(3)	5.118(24)	12.0(2)	10.431(9)
866	0.405(5)	5.358(37)	21.6(3)	10.755(13)
867	0.563(7)	5.582(62)	31.2(5)	11.048(21)
868	1.238(14)	6.549(35)	80.7(12)	12.270(30)

C. Compressive strength

The elastic precursor manifests itself as a sharp jump in velocity which relaxes by up to 25% (Fig. 2). Under a steady-wave assumption, the amplitude of the Hugoniot elastic limit can be obtained from:

$$\sigma_{\rm HEL}=\frac{\rho_0 V_{P0}u_{\rm fs}}{2}, \tag{4}$$

where the factor-of-two relationship between the free surface and particle velocity has been assumed.[17] The measured HEL stresses are listed in Table III.

No peak stress dependence of the HEL amplitude can be resolved over the 12–31 GPa stress range of the present experiments (Fig. 5). Wave profiles measurements on molybdenum between 7 and 15 GPa from a 25 °C initial state have recently been reported.[3] Hugoniot elastic limit values of 2.3–2.8 GPa were obtained for sample thicknesses between 1.5 and 13 mm. At 1400 °C, the HEL amplitude of Mo is therefore reduced by 26%–46% relative to its room temperature value. This contrasts with observations for bismuth[18] in

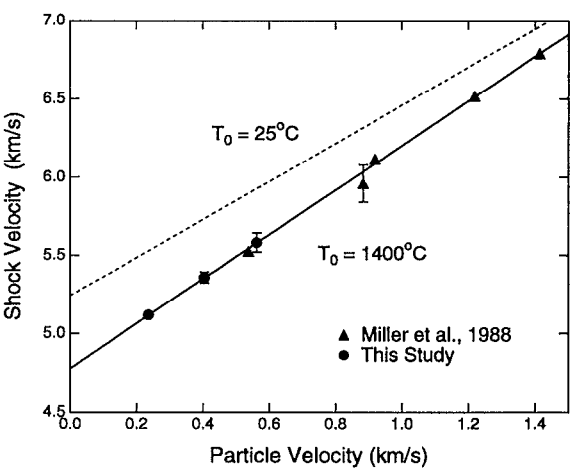

FIG. 4. Shock velocity-particle velocity data for Mo shocked at 1400 °C. The error bars are smaller than the symbols where not shown. The solid curve is a weighted least-squares fit to the 1400 °C data. The dashed curve is the 25 °C Hugoniot from Ref. 40.

TABLE III. Constitutive and elastic properties of molybdenum shock compressed from a 1400 °C initial state.

Shot	σ_{HEL} (GPa)	Y_0 (GPa)	V_P (km/s)	T_H (°C)	$\lvert(\partial V_P/\partial T)_P\rvert$ (m/s/°C)	ν
865	1.73(7)	0.94(5)	6.30(22)	1532(22)	0.35(13)	0.34(3)
866	1.46(7)	0.79(5)	6.72(12)	1642(37)	0.24(9)	0.33(2)
867	1.73(7)	0.94(5)	7.07(21)	1753(57)	0.16(13)	0.33(3)
868	···	···	7.91(24)	2448(186)	0.18(11)	0.38(3)

which the precursor amplitude was independent of temperature up to 250 °C, which is near the melting temperature for that material.

Another interesting feature of the elastic precursor structure is the decrease in free surface velocity behind the precursor, which at its minimum is 74%–88% of the peak precursor velocity. Elastic wave overshoot has previously been identified in other materials[19] and is interpreted as a consequence of stress relaxation. Room-temperature free surface and particle velocity profiles in Mo, however, show no stress relaxation behind the precursor.[3,4] Therefore, the high initial temperature both decreases the magnitude of the HEL and promotes stress relaxation behind the precursor. These results are somewhat anomalous in that reduction of velocity behind the HEL is observed, but no dependence of the HEL amplitude on peak driving stress can be resolved. Both these phenomena are generally associated with stress relaxation in solids.[20,21] It may be that the present data are insufficient to resolve the peak-stress dependence of the HEL.

Assuming a von Mises yield condition, the compressive yield strength, Y_0, is related to the HEL amplitude through:

$$Y_0=\frac{(1-2\nu)}{(1-\nu)}\,\sigma_{HEL}, \tag{5}$$

where ν is Poisson's ratio. At 1400 °C, Poisson's ratio is estimated to be 0.313 from extrapolation of ultrasonic elasticity data.[15] The resulting yield strengths are listed in Table III and plotted as a function of initial temperature in Fig. 6.

In recent constitutive models,[4,11] thermal effects are incorporated by assuming that the ratio Y/G is constant, where G is the shear modulus. An alternative representation is that the yield strength is the following function of homologous temperature:

$$Y_0=1.59(1-T/T_m), \tag{6}$$

where T_m is the melting temperature (in K). This equation was obtained using the 25 °C yield strength and requiring that Y=0 GPa at the melting temperature. This is similar to a previous relationship[22] in which the yield strength depends on the ratio of internal energy to the melt energy. The experimental data fall in between the predictions of these two relations (Fig. 6). The yield strength at the HEL decreases more rapidly than the shear modulus but more slowly than predicted by Eq. (6).

D. Unloading wave velocities

The time difference, Δt, between the arrival of the unloading wave and the arrival of either the shock or elastic precursor at the free surface was measured from the wave profiles or the fringe records. The Lagrangian unloading velocity, V_{PL}, in the sample is then given by (cf. Fig. 3):

$$V_{PL}=\frac{x_s-h^*}{\Delta t+x_s/U_1-x_f(1/U_{Sf}+1/V_{PLf})-h^*/V^*}, \tag{7}$$

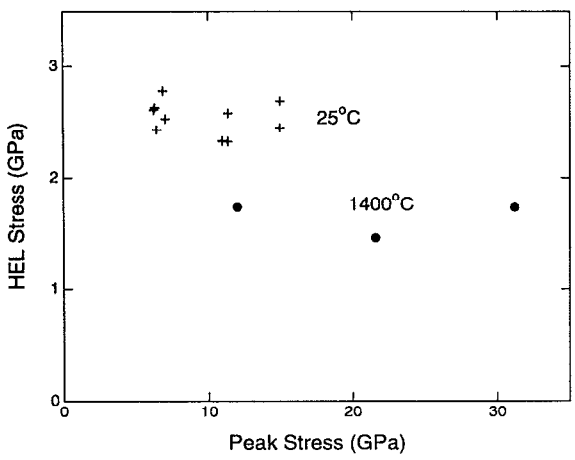

FIG. 5. Hugoniot elastic limit stress as a function of peak stress in Mo. The filled circles are the present data (initial temperatures near 1400 °C). The pluses are measured from a 25 °C initial state (Ref. 3).

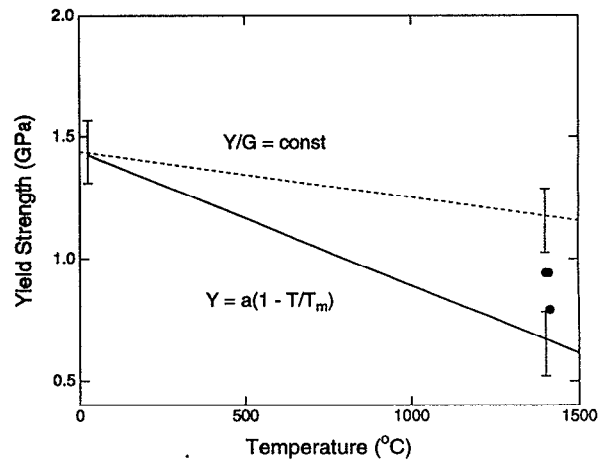

FIG. 6. Yield strength of molybdenum as a function of initial temperature. Solid symbols are data of this study. Error bars on solid and dashed lines show the range of values from Ref. 3.

TABLE IV. Equation of state and constitutive properties of materials used in molybdenum experiments. c_0 and s are the Hugoniot EOS constants.

Material	ρ_0 (g/cm^3)	c_0 (km/s)	s	γ_0	ν_0	Y_0 (GPa)	Refs.
Mo (25 °C)	10.21(1)	5.136(16)	1.220(10)	1.52	0.293	1.4	40
Mo (1400 °C)	9.95(1)	4.78(2)	1.42(2)	1.52	0.313	0.9	5, this study
Al 6061	2.69(1)	5.349(56)	1.338(20)	2.1	0.34	0.2	40
Ta	16.58(7)	3.293(5)	1.307(25)	1.6	0.34	0.8	41

where x_s and x_f are the sample and flyer thicknesses, U_{Sf} and V_{PLf} are the shock velocity and the Lagrangian unloading velocity in the flyer, U_1 is either the shock or precursor velocity in the sample depending on how Δt is measured, and V^* is the average velocity in the perturbed region, h^*, which is defined by the intersection of the unloading wave from the back of the flyer and the unloading wave from the free surface:

$$h^* = \frac{V_{PL}}{2}[x_f(1/V_{PLf} + 1/U_{Sf}) + x_s(1/V_{PL} - 1/U_S)]. \tag{8}$$

In the interaction region, the unloading wave travels through a non-simple region of near zero stress before reaching the free surface. The initial bulk sound velocity, V_{B0}, was used as an estimate of the average velocity, V^*, in this region. The interaction region was restricted to less than 10% of the sample thickness to minimize its effect on the unloading wave velocities. The large stress drop in this region could be minimized if a window were attached to the sample rear surface. We have not developed a window-attachment method that can withstand the high-temperature environment of the present experiments.

Equations (7) and (8) were solved iteratively for V_{PL}. Hugoniot states in the flyer materials were determined through impedance matching[23] using the parameters of Table IV. Unloading wave velocities in aluminum 6061 to 41 GPa have been determined in previous work[24,25] and can be described by the expression

$$V_P = 1.8796 + 0.0303 \ln \sigma + 0.0177(\ln \sigma)^2, \tag{9}$$

where σ is the stress in GPa. V_P is the Eulerian unloading velocity (in km/s) and is related to the Lagrangian value by

$$V_P = \frac{\rho_0}{\rho} V_{PL}. \tag{10}$$

For experiment 868, the Hugoniot stress (80.7 GPa) is close to a previously reported 83.1 GPa experiment[26] for which a Ta unloading velocity of 5.5(2) km/s was measured. This value was used in Eqs. (7) and (8) for this experiment. The Eulerian unloading velocities for Mo are listed in Table III and plotted as a function of Hugoniot stress in Fig. 7.

For solids in the absence of dispersion, the initial unloading wave velocity corresponds to the compressional elastic wave velocity, V_P, while for liquids it corresponds to the bulk wave velocity, V_B.[14] The identification of the initial unloading velocity with the compressional sound velocity is supported by comparisons of Hugoniot and extrapolated ultrasonic data at low pressures where thermal effects are small.[27] On the other hand, micromechanical theory has been used to suggest that due to immediate reverse plastic flow, the observable release may not always correspond to fully elastic behavior.[28] This effect is not expected to be significant in BCC metals such as molybdenum, however.[29]

The measured sound velocities lie well above extrapolated bulk velocities, indicating that Mo remains solid over the range of the present experiments. The velocities are 4%–8% below 25 °C wave profile data and extrapolated ultrasonic data. This reflects the effect of temperature on the compressional wave velocity. The temperature coefficient of compressional velocity, $(\partial V_P/\partial T)_P$, can be calculated from

$$\left(\frac{\partial V_P}{\partial T}\right)_P \approx \frac{V_{PH} - V_{PI}}{T_H - T_I}, \tag{11}$$

where T is the temperature, and the subscripts H and I represent conditions on the Hugoniot and isotherm, respectively. Sound velocities along the reference 25 °C isotherm were computed using third-order Eulerian finite-strain theory[30] and ultrasonic elastic moduli and pressure derivatives of Mo.[31] The difference between the Hugoniot stress and mean

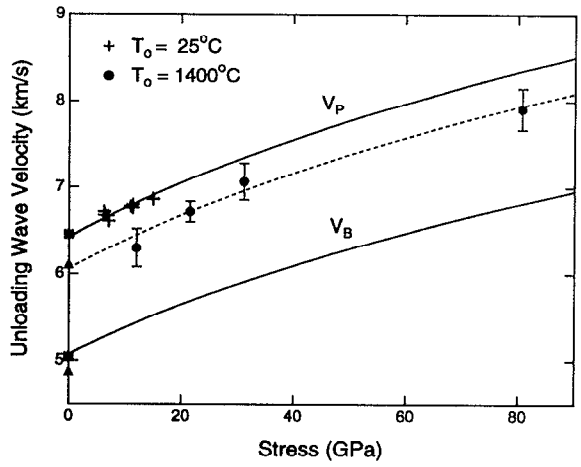

FIG. 7. Unloading wave velocity in Mo as a function of Hugoniot stress. Solid circles are the present results (1400 °C). The squares and triangles are the ambient-pressure compressional and bulk sound speeds at 25 °C and 1400 °C, respectively. Pluses are calculated from the wave profiles (25 °C) of Ref. 3. The solid curves are third-order Eulerian finite-strain extrapolations of compressional and bulk sound velocities at room temperature. The dashed line is a fit to the high T data using Birch's law and the Hugoniot equation relating stress and density.

pressure has been neglected in this analysis. The calculated isotherm velocities are consistent with values at 7–15 GPa from a 25 °C initial state obtained from previous wave profiles[3] (Fig. 7).

Hugoniot temperatures were calculated by solving the following equation[32]:

$$V\frac{dT}{dV} = -\gamma T + \left(\frac{V}{2C_V}\right)\left[\frac{dP}{dV}(V_0 - V) + P\right], \tag{12}$$

where V is the specific volume, C_V is the constant volume specific heat, and γ is the Grüneisen parameter. Values of γ and C_V for 1400 °C Mo were taken from Ref. 5, and the difference between the isobaric and isochoric specific heats has been neglected. Both C_V and the product, $\rho\gamma$, were assumed constant along the Hugoniot.

The quantities calculated using Eqs. (11) and (12) are listed in Table III. Within their uncertainties, high-pressure values of the temperature coefficient of compressional velocity are consistent with the ambient-pressure value of $(\partial V_P/\partial T)_P = -0.247$ m/s/°C.[15] There is also a general trend toward decreasing values with increasing pressure. This has been observed for a number of other metals from room temperature shock compression.[33]

While the present results are consistent with previous analyses, the method used here offers significant advantages for constraining temperature derivatives. The shock temperature rise is relatively small compared with the precisely known initial temperature, significantly reducing uncertainty in the final temperatures. The high initial temperature also allows comparison of shock and ultrasonic data at relatively low pressure (~10 GPa). This reduces uncertainty associated with extrapolation of ultrasonic data to very high pressure. For these reasons, it is felt that the present results are less likely to suffer from systematic biases than the previous analysis.

Sound velocities measured in Mo shock compressed to between 150 and 441 GPa from a 25 °C initial state have also been reported.[8] A solid-solid transition at about 210 GPa and melting at about 390 GPa were identified from this data. The solid-solid transformation was interpreted as a bcc to hcp transition caused by $s \rightarrow d$ electronic transfer. Figure 8 shows a comparison of all Hugoniot sound velocity data for Mo. The data between 150 and 210 GPa are anomalous in that they imply large values of Poisson's ratio which decrease across this pressure interval whereas Poisson's ratio generally increases with both pressure and temperature. This, together with a softening of the EOS, has also been interpreted as a consequence of the $s \rightarrow d$ electronic transfer which begins above 100 GPa.[9]

We see no evidence of anomalous behavior in V_P up to 81 GPa from our high-temperature initial state. The Hugoniot velocities are subparallel to extrapolated ultrasonic data (Figs. 7 and 8). This is consistent with behavior observed in shock data for several other metals[33] and can be attributed to thermal effects. In contrast, the present data appear inconsistent with the 25 °C initial temperature data shocked to 150–210 GPa. These sound velocities may be strongly influenced by the proposed electronic transfer. The possibility of a second solid-solid phase change at pressures between 81 and 150 GPa must also be considered. Under static compression, no phase transformations were observed in Mo to at least 272 GPa.[7]

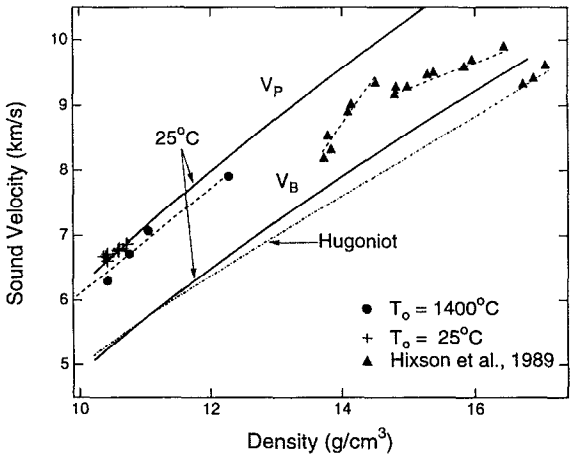

FIG. 8. Sound velocities in Mo as a function of density. Solid lines show finite-strain extrapolations of low-P ultrasonic data. The dash-dot line is the bulk sound velocity computed from the Hugoniot slope. Dashed lines are linear fits to data from 0–81 GPa (T_0=1400 °C), 150–210 GPa, and 210–390 GPa. Filled circles—this study; pluses—computed from wave profiles of Ref. 3; triangles—Ref. 8.

Compressional and bulk sound velocity data for many metals satisfy Birch's Law over broad shock compression intervals.[27,34] That is, velocity is a linear function of density with a slope dependent upon atomic weight. The Mo data between 150 and 210 GPa do not extrapolate linearly in density to the ambient-pressure compressional velocity. However, the 1400 °C data to 81 GPa approximately satisfy Birch's law. Linear velocity-density fits are shown in Fig. 8, together with ultrasonic extrapolations and bulk sound speeds calculated from the Hugoniot slope.

Poisson's ratio, ν, can be computed by combining measured compressional velocities with bulk velocities constrained by the Hugoniot slope and the assumption that $\rho\gamma$ = const.[8,32] Poisson's ratio values for Mo are listed in Table III. The ambient-pressure 1400 °C value of ν from extrapolation of ultrasonic data is 0.313, as discussed previously. These data indicate that Poisson's ratio increases along the Hugoniot over this pressure range. Increases in ν have been documented for other metals under Hugoniot conditions.[27]

E. Estimated spall strength

The interaction of unloading waves depicted in Fig. 3 leads to dynamic fracture or spall. The characteristic signature of spall is an increase or pull-back in free surface velocity as seen in Fig. 2. From the amplitude of the pull-back signal, an estimate of the spall strength can be obtained. For an elastic-plastic material, the spall strength, S, is given by[16,35]

$$S = S_{fs} + \Delta S, \tag{13}$$

where S_{fs} is the amplitude of the tensile-stress pulse recorded at the free surface

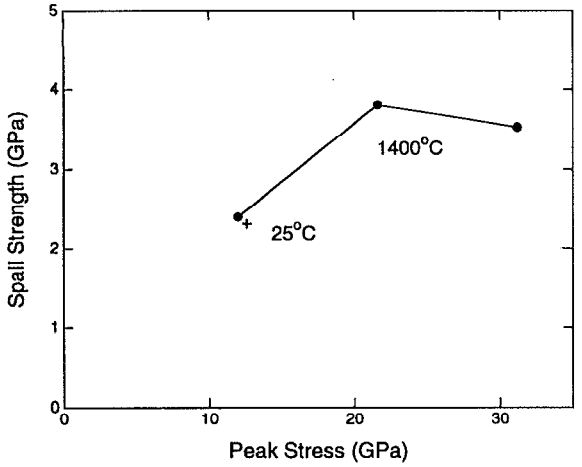

FIG. 9. Estimated spall strength of Mo as a function of peak stress. Solid symbols are high-temperature results. Plus symbol is from room-temperature data (Ref. 36).

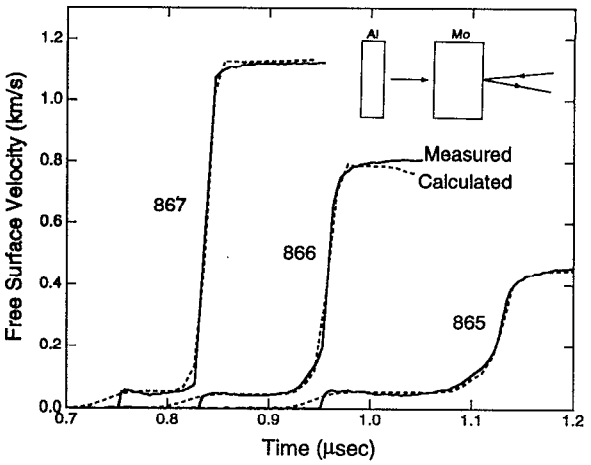

FIG. 10. Comparison of measured shock waveforms in 1400 °C preheated Mo with finite-difference simulations. The solid lines show the measured waveforms and the dashed lines are computer simulations using the WONDY code. The starting times of the waveforms are arbitrary and offset for clarity.

$$S_{fs}=\tfrac{1}{2}\rho_0 V_P \Delta u_{pb}, \tag{14}$$

where Δu_{pb} is the pull-back amplitude measured from the peak free surface velocity to the velocity minimum. The term ΔS accounts for the attenuation of the spall signal in propagating from the spall plane to the free surface:

$$\Delta S=\frac{S_{fs}\delta}{\tau}\left(\frac{1}{V_B}-\frac{1}{V_P}\right), \tag{15}$$

where τ is the pull-back pulse duration, and δ is the distance to the spall plane which we have assumed is equal to h^*. The resulting estimated spall strengths for Mo between 12 and 31 GPa are shown in Fig. 9. Near 12 GPa, the spall strength of 1400 °C Mo is 2.4 GPa, not significantly different from the value of 2.31 GPa reported for room-temperature Mo at this stress.[36] Thus, in contrast to the compressive yield strength, the spall strength appears to be only weakly dependent on temperature for this material. Similar results have been obtained for copper pre-heated to 425 °C.[37] The spall strength shows a tendency to increase with increasing peak stress as has also been observed in other materials.[16]

F. Modeling

Computer simulations of the present experiments were undertaken using the one-dimensional finite-difference wavecode WONDY.[38] Both Mo and aluminum 6061 were modeled as elastic-perfectly plastic materials (Table IV). The results of the simulations are shown in Fig. 10 and are in good agreement with the experimental profiles. The primary feature to note is that the rise time of the plastic shock front is significantly greater at low stress and is approximately 50 ns for the 12 GPa experiment.

EOS experiments on high-temperature liquid silicates encapsulated in Mo have yielded important insights into magma petrogenesis.[6,39] We have performed additional wavecode simulations in order to investigate the expected shock structure in such experiments. The computer simulations consisted of aluminum 6061 impactors traveling at 1 and 2.5 km/s impacting a 0.76-mm Mo driver plate behind which was a 3.3-mm thick layer of liquid silicate followed by a 2.0-mm thick Mo cap. A liquid silicate of komatiite composition was used in the simulations.[39] These impacts produce peak stresses of 5.6 and 18.4 GPa in the liquid silicate sample and 10.2 GPa and 33.1 GPa in the Mo cover plate, respectively.

The compressive waveforms from the simulations are shown in Fig. 11 as well as waveforms from identical simulations in which the Mo-silicate sandwich is replaced by a single Mo layer of equal thickness. For the 2.5 km/s simulation, the compressive waveforms with and without the komatiite layer are similar. For the lower velocity simulation, significant additional structure is introduced by wave interactions generated at the silicate/Mo interface. These results

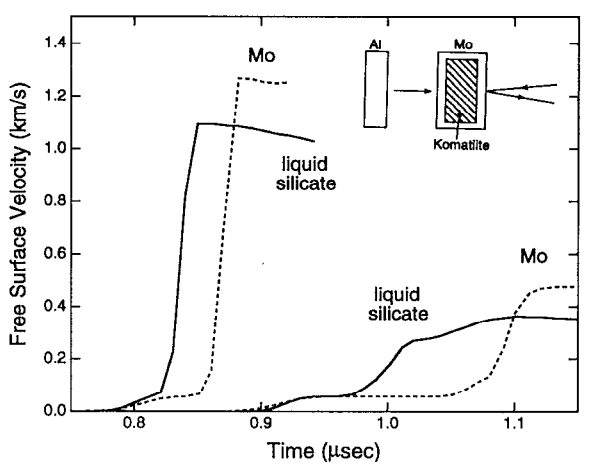

FIG. 11. Calculated free surface velocity profiles for molten-silicate experiments (see Refs. 6 and 39) conducted in our laboratory based on computer simulations. The solid curves show calculated compressive-wave structure for a komatiite sample encapsulated by Mo and impacted with an Al 6061 flyer at 2.5 km/s (left) and 1.0 km/s (right). The dashed curves show the same simulations except that the komatiite layer has been replaced by Mo.

suggest that EOS experiments on liquid silicates using streak camera detection may be ambiguous at low shock stresses (<5 GPa) because of the long rise time of the plastic wave front and the broadening of the shock front that arises due to wave interactions. This may explain the failure of shock transit time measurements in liquid silicates at low stresses.[39]

IV. SUMMARY

VISAR wave profile measurements on shocked solids have been extended to materials at very high initial temperature. This opens up new opportunities for measuring material strength, sound velocities, and melting phenomena at high-temperature states off the principal Hugoniot. Initial experiments on molybdenum shock loaded at 1400 °C yield the following results:

(1) The equation of state of 1400 °C molybdenum from VISAR and shock transit time measurements can be expressed as:

$$U_S = 4.78(2) + 1.42(2)u_p,$$

for particle velocities between 0.236 and 1.414 km/s. The bulk sound velocity at 1400 °C from linear extrapolation of ultrasonic data is 4.88 km/s, in reasonable agreement with the Hugoniot equation of state intercept.

(2) The effect of 1400 °C initial temperature is to reduce the Hugoniot elastic limit by about one-third relative to its room temperature value. Stress relaxation behind the precursor is observed in the high initial temperature experiments but not in previous room-temperature experiments. The yield strength at the elastic limit decreases with temperature at a rate of $4(1)\times10^{-4}$ GPa/°C.

(3) Unloading wave velocities range from 6.3 km/s at 12 GPa to 7.91 km/s at 80.7 GPa. These are 4%–8% below velocities obtained from room temperature shock compression and extrapolation of ultrasonic data. Values of the temperature coefficient of compressional velocity between −0.35(13) m/s/°C and −0.16(13) m/s/°C were obtained from comparison with ultrasonic data.

(4) The estimated spall strength of 1400 °C Mo is 2.4–3.8 GPa at stresses between 12 and 31 GPa. No temperature dependence of the spall strength can be resolved from currently available data.

(5) The rise time of the shock front decreases rapidly with increasing stress. Wavecode simulations of liquid silicate experiments indicate that shock transit time measurements at low stresses (<5 GPa) may not be reliable because of long risetimes and wave interactions.

ACKNOWLEDGMENTS

We thank L. Rowan, E. Gelle, M. Long, and A. DeVora for experimental assistance and O. B. Crump and L. Barker of Sandia National Labs for technical advice. M. Furnish of Sandia provided us with copies of his data. This research was supported by the NSF. Contribution 5348, Division of Geological and Planetary Sciences, California Institute of Technology.

[1] L. M. Barker and R. E. Hollenbach, J. Appl. Phys. **43**, 4669 (1972).
[2] R. S. Hixson and J. N. Fritz, J. Appl. Phys. **71**, 1721 (1992).
[3] M. D. Furnish and L. C. Chhabildas, in *High Strain Rate Behavior of Refractory Metals and Alloys*, edited by R. Asfahani, E. Chen, and A. Crowson (The Minerals, Metals, and Materials Society, Warrendale, PA, 1992), p. 229.
[4] D. J. Steinberg, J. Appl. Phys. **74**, 3827 (1993).
[5] G. H. Miller, T. J. Ahrens, and E. M. Stolper, J. Appl. Phys. **63**, 4469 (1988).
[6] S. M. Rigden, T. J. Ahrens, and E. M. Stolper, J. Geophys. Res. **93**, 367 (1988).
[7] Y. K. Vohra and A. L. Ruoff, Phys. Rev. B **42**, 8651 (1990).
[8] R. S. Hixson, D. A. Boness, J. W. Shaner, and J. A. Moriarty, Phys. Rev. Lett. **62**, 637 (1989).
[9] B. K. Godwal and R. Jeanloz, Phys. Rev. B **41**, 7440 (1990).
[10] J. R. Asay and G. I. Kerley, Int. J. Impact Eng. **5**, 69 (1987).
[11] D. J. Steinberg, S. G. Cochran, and M. W. Guinan, J. Appl. Phys. **51**, 1498 (1980).
[12] T. J. Ahrens, J. H. Lower, and P. L. Lagus, J. Geophys. Res. **76**, 518 (1971).
[13] W. Hemsing, High Speed Photogr. Videogr. and Photon. **427**, 199 (1983).
[14] Ya. B. Zel'dovich and Yu. P. Raizer, *Physics of Shock Waves and High-Temperature Hydrodynamic Phenomena* (Academic, New York, 1967).
[15] J. M. Dickinson and P. E. Armstrong, J. Appl. Phys. **38**, 602 (1967).
[16] D. E. Grady, in *Metallurgical Applications of Shock-Wave and High Strain Rate Phenomena*, edited by L. E. Murr, K. P. Staudhammer, and M. A. Meyers (Marcel Dekker, New York, 1986), p. 763.
[17] J. M. Walsh, M. H. Rice, R. G. McQueen, and F. L. Yarger, Phys. Rev. **108**, 196 (1957).
[18] J. R. Asay, J. Appl. Phys. **45**, 4441 (1974).
[19] L. M. Barker and R. E. Hollenbach, J. Appl. Phys. **45**, 4872 (1974).
[20] T. J. Ahrens and G. E. Duvall, J. Geophys. Res. **71**, 4349 (1966).
[21] R. A. Graham and W. P. Brooks, J. Phys. Chem. Solids **32**, 2311 (1971).
[22] L. J. Hageman and J. M. Walsh, Systems, Science, and Software Report No. 3SR-350, La Jolla, CA, 1970.
[23] T. J. Ahrens, in *Methods of Experimental Physics*, edited by C. G. Sammis and T. L. Henyey (Academic, San Diego, CA, 1987), Vol. 24, p. 185.
[24] J. R. Asay and L. C. Chhabildas, in *Shock Waves and High Strain-Rate Phenomena in Metals*, edited by M. A. Meyers and L. E. Murr (Plenum, New York, 1981), p. 417.
[25] T. S. Duffy and T. J. Ahrens (unpublished data).
[26] J. R. Asay, L. C. Chhabildas, G. I. Kerley, and T. G. Trucano, in *Shock Waves in Condensed Matter—1985*, edited by Y. M. Gupta (Plenum, New York 1986), p. 145.
[27] T. S. Duffy and T. J. Ahrens, in *High-Pressure Research in Mineral Physics: Applications to Earth and Planetary Sciences*, edited by Y. Syono and M. H. Manghnani (Terra Scientific, Tokyo, 1992), p. 353.
[28] J. N. Johnson, J. Phys. Chem Solids **54**, 691 (1993).
[29] J. N. Johnson, R. S. Hixson, D. L. Tonks, and G. T. Gray, Bull. Am Phys. Soc. **38**, 1511 (1993).
[30] C. Sammis, D. Anderson, and T. Jordan, J. Geophys. Res. **75**, 4478 (1970).
[31] K. W. Katahara, M. H. Manghnani, and E. S. Fisher, J. Phys. F: Metal Phys. **9**, 773 (1979).
[32] R. G. McQueen, S. P. Marsh, J. W. Taylor, J. N. Fritz, and W. J. Carter, in *High-Velocity Impact Phenomena*, edited by R. Kinslow (Academic, New York, 1970), p. 294.
[33] T. S. Duffy and T. J. Ahrens, J. Geophys. Res. **97**, 4503 (1992).
[34] J. W. Shaner, J. Chem. Phys. **89**, 1616 (1988).
[35] V. I. Romanchenko and G. V. Stepanov, Zhur. Prik. Mekh. Tekh. Fia. **4**, 141 (1980).
[36] L. C. Chhabildas, L. M. Barker, J. R. Asay, and T. G. Trucano, Int. J. Impact Eng. **10**, 107 (1990).
[37] S. J. Bless and D. L. Paisley, in *Shock Waves in Condensed Matter—1983*, edited by J. R. Asay, R. A. Graham, and G. K. Straub (Elsevier, New York, 1984), p. 163.
[38] M. E. Kipp and R. J. Lawrence, Sandia National Lab. Report No. SAND81-0930, Albuquerque, NM, 1982.
[39] G. H. Miller, E. M. Stolper, and T. J. Ahrens, J. Geophys. Res. **96**, 11 831 (1991).
[40] S. P. Marsh, *LASL Shock Hugoniot Data* (University of California Press, Berkeley, 1980).
[41] A. C. Mitchell and W. J. Nellis, J. Appl. Phys. **52**, 3363 (1981).